Chemical Engineering Journal 156 (2010) 170–176

Contents lists available at ScienceDirect

Chemical Engineering Journal

journal homepage: www.elsevier.com/locate/cej

Characterization of nanofibrous carbon produced at pilot-scale in a fluidized bed reactor by methane decomposition

J.L. Pinilla[a], M.J. Lázaro[a], I. Suelves[a,*], R. Moliner[a], J.M. Palacios[b]

[a] Instituto de Carboquímica, CSIC, Miguel Luesma 4, 50018 Zaragoza, Spain
[b] Instituto de Catálisis y Petroleoquímica, CSIC, Campus Universidad Autónoma, Cantoblanco, 28049 Madrid, Spain

ARTICLE INFO

Article history:
Received 2 July 2009
Received in revised form 1 October 2009
Accepted 8 October 2009

Keywords:
Fluidized bed reactor
Carbon nanofiber
Hydrogen production
Methane catalytic decomposition

ABSTRACT

Carbon nanofibers (CNFs) production in the range of hundreds of grams per day has been achieved in a fluidized bed reactor (FBR) by methane decomposition using a nickel based catalyst. The characterization of the carbon produced at different operating conditions (temperature, space velocity and the ratio of gas flow velocity, u_o, to the minimum fluidization velocity, u_{mf}) has been accomplished by means of X-ray diffraction (XRD), N_2 adsorption, temperature-programmed oxidation (TPO), scanning electron microscope (SEM) and transmission electron microscopy (TEM). It has been concluded that the structural and textural properties of the CNFs obtained in the FBR are analogous to the ones obtained in a fixed bed reactor at a production scale two orders of magnitude lower. Thus, FBR can be envisaged as a promising reaction configuration for the catalytic decomposition of methane (CDM), allowing the production of high quantities of CNFs with desirable structural and textural properties.

1. Introduction

The catalytic decomposition of methane (CDM) into hydrogen and carbon is an interesting alternative to other conventional hydrogen production methods because it does not yield CO_2 [1,2]. In the CDM process using nickel catalysts, carbon is mostly captured as a solid of a high added value in the form carbon nanofibers (CNFs). CNFs are made of graphenes, existing in a graphitic carbon structure, aligned along different directions referred to the fiber axis. CNFs are products finding multiple uses, such as catalyst support [3], mechanical reinforcement component in carbon composites [4], electrode material [5], graphite material precursor [6], etc. A widely accepted mechanism for CNFs formation includes the decomposition of the methane previously chemisorbed on faces (1 0 0) and (1 1 0) of nickel nanoparticles to form atomic carbon that rapidly diffuse toward Ni faces (1 1 1) in which is deposited growing into nanofibers of different structures [7].

The production at large-scale of these carbon materials is currently a key point for the commercial application of the CDM process, and it is highly related to the type of reactor used [8]. There is a need of developing suitable reactor configurations in order to overcome the blocking problems associated to the fixed bed operation, in which the great amount of carbon deposited provokes the agglomeration of the bed of particles. Recently, various kinds of reactor configuration have been proposed as a viable alternative for the large-scale production of hydrogen and CNF. For instance, the use of rotary bed reactors for the CDM process has been carried out in [9,10].

Lastly, great attention has been devoted to the study of fluidized bed reactors (FBR) for large-scale production of carbon nanotubes [11,12] and for the simultaneous production of hydrogen and nanostructured carbon by means of CDM [13–17].

According to Vahlas et al. [18], some of the main potential advantages of using a FBR for the catalytic decomposition of hydrocarbons are (i) to ensure efficient mixing of the grains in the bed and efficient mass transfer through large exchange surfaces between the gaseous carbon source and the catalyst grains and (ii) to ensure an almost uniform temperature in the reaction zone. Additionally, from the industrial point of view, this reactor configuration allows to carry out the operation in a continuous mode, by adding fresh catalyst and withdrawing simultaneously the carbon produced together with the exhausted gases.

As regards the CNF applications, the influence of the operational conditions, such as temperature, space velocity or the ratio of gas flow velocity, u_o, to the minimum fluidization velocity, u_{mf}, on the CNF characteristics should be taken into account in order to select the most adequate conditions in the CDM reactor allowing to produce simultaneously high methane conversions.

In a previous work our research group designed and built up an FBR semi-pilot plant capable of producing in discontinuous mode, up to hundreds of grams per day of carbon nanofibers and m^3/day of H_2 [17]. The influence of the operational parameters on the perfor-

* Corresponding author. Fax: +34 976 73 3318.
E-mail address: isuelves@icb.csic.es (I. Suelves).

1385-8947/$ – see front matter © 2009 Elsevier B.V. All rights reserved.
doi:10.1016/j.cej.2009.10.032

mance of a NiCu/Al_2O_3 catalyst was also studied [19,20], showing that hydrogen production was enhanced by increasing operating temperature and lowering space velocity. However, an increase in operating temperature, space velocity and the ratio of gas flow velocity, u_o, to the minimum fluidization velocity, u_{mf} (u_o/u_{mf}) provoked an increase in the catalyst deactivation rate. In an attempt to expand our previous work, here we focus on the main physicochemical properties of nanofibrous carbon obtained in the CDM reaction tests before mentioned using a NiCu based catalyst in a FBR, by varying the reaction conditions (temperature, space velocity and the ratio u_o/u_{mf}). Additionally, a typical as produced carbon material is compared to that obtained under the same operational conditions at a fixed bed reactor.

2. Experimental

2.1. Catalyst and experimental set-up

The catalyst denoted as NiCu/Al_2O_3 was prepared by the fusion method following the procedure previously described [21,22]: a catalyst with NiCu/Al_2O_3 of 78/6/16 ratio in their respective components was prepared by fusing nitric salt of nickel and copper nitrate with nitric salt of aluminium followed by decomposition of the mixtures at 350 °C and subsequent calcination at 450 °C. The respective powder X-ray diffraction (XRD) patterns indicated that NiO was the only crystalline phase present in the fresh calcined catalysts with a crystal domain size of 23 nm, which was proven to promote the carbon deposition as very long nanofibers in a reaction test [23]. Further details regarding catalyst characterization can be found elsewhere [21,22]. The CDM tests were carried out in a fluidized bed reactor (dimensions: 0.80 m height, 0.065 m diameter) described in detail in [17].

2.2. Operating conditions for CNF synthesis

All experiments were conducted at atmospheric pressure. In a typical experiment, the amount of catalyst (10 g) was placed in the reactor and nitrogen was flown while temperature was raised up to 550 °C. Then, the catalyst was subjected to a reduction treatment by using a flow rate of pure hydrogen of 80 l/h for 3 h. Afterwards, nitrogen was again flown while the desired reaction temperature was reached. Finally, pure methane (99.99%) was fed into the reactor for methane decomposition at the selected operating temperature. The methane flow rate was adjusted in each case in order to get the desired weight hourly space velocity (WHSV, defined here as methane flow rate at standard conditions per mass of fresh catalyst initially loaded).

Several tests were performed in order to evaluate the influence of the operating conditions on the characteristics of the carbon nanofibers. The influence of the temperature was studied by varying it in the range 600–800 °C, while keeping a constant WHSV of 12 l/(g_{cat} h). The influence of the space velocity was studied in the range of 4–24 l/(g_{cat} h), while keeping a constant reaction temperature of 700 °C. Lastly, the influence of the ratio u_o/u_{mf} was studied in the range 2–6, at a reaction temperature of 700 °C and space velocity of 8 l/(g_{cat} h). The changes in the u/u_{mf} while keeping constant the WHSV were performed by fixing the methane flow rate corresponding to the desired ratio u_o/u_{mf}, and adjusting in each case the amount of catalyst initially loaded in the reactor to get the desired WHSV.

The carbon deposited during each run (C_{dep}) was determined by direct weight and confirmed by applying the carbon mass balance between the methane fed to the reactor and the un-reacted methane, measured by means of a micro-GC, within an error lower than 5%. The average carbon deposition rate (R_w) denoted the amount of carbon deposited per gram of catalyst initially loaded and per hour (g C/(g_{cat} h)). The minimum fluidization velocity (u_{mf}) was calculated by the method proposed by Wen and Yu [24].

2.3. Characterization techniques

The textural properties of the CNFs were measured by N_2 adsorption at 77 K in a Micromeritics ASAP2020 apparatus. The specific surface areas and pore volumes were calculated by applying the BET method to the respective N_2 adsorption isotherms.

XRD patterns of fresh and used samples were acquired in a PANalytical diffractometer using a θ–2θ configuration, Ni-filtered Cu Kα radiation and a secondary graphite monochromator. The angle range scanned was 10–100° using a counting step of 0.02° and a counting time per step of 20 s. A suitable sample holder with a very low noise level was used, allowing for pattern acquisitions from a small amount of sample with good resolution. The powder XRD patterns were further processed using the accompanying X'Pert Highscore Plus software to obtain refined structural parameters for the desired compounds through the application of Rietveld methods.

Temperature-programmed oxidation (TPO) profiles of the used samples in FBR tests were obtained in a Setaram Thermogravimetric Analyzer carried out under air atmosphere using a heating rate of 10 °C/min.

The morphological appearance of the deposited carbon was studied with an electron microscope (SEM) (Hitachi S-3400) coupled to a Si/Li detector for energy dispersive X-ray (EDX) analysis.

The transmission electron microscopy (TEM) study has been performed in a JEOL 2010 microscope provided with a field emission electron source working in image mode and using an accelerating voltage of 200 kV. TEM samples were prepared by the usual method of dispersing a small amount of powder sample in ethanol, stirring in an ultrasonic apparatus for 10 min, allowing the homogenized liquid to settle for 3 min and, taking a drop from the top of the liquid-containing vessel to a conventional TEM holder consisting of a membrane of amorphous carbon supported on a Cu grill of 3 mm in diameter. TEM micrographs were taken from selected areas of interest in the sample, which were sufficiently thin to achieve the desired high resolution.

The mean particle diameter of the carbon product obtained by CDM was determined by laser diffraction (Beckman-Coulter LS 13 320).

Bulk densities, ρ_b, was calculated by measuring the mass of a known volume of particles placed inside a graduated cylinder, without packing down the particles.

3. Results

3.1. CNF production

The influence of the studied variables (temperature, space velocity and the ratio u_o/u_{mf}) on the hydrogen production and on the methane decomposition rate was the subject of previous works [19,20]. Table 1 shows the NiCu/Al_2O_3 catalyst performance in terms of both products obtained as results of methane decomposition reaction: CNF and hydrogen. Thus, Table 1 summarizes the CNF yield and CNF average formation rate (R_w) in reactor tests carried out under different operating conditions. Table 1 also includes kinetics data extracted from [19,20]: the initial hydrogen concentration (measured after 10 min time on stream) and the average methane conversion. Additionally, the catalyst deactivation expressed by means of the sustainability factor (defined as the ration between the initial methane decomposition rate and the

Table 1
Initial hydrogen concentration ($H_{2,0}$), average methane conversion (χ_{CH_4}), sustainability factor (r_5/r_0), CNF production and average deposition rate (R_w) at different operating conditions used for the CNF synthesis in a FBR.

T (°C)	WHSV (l/(g_{cat} h))	u_o/u_{mf}	Run time (min)	$H_{2,0}$ (vol.%)	χ_{CH_4} (%)	r_5/r_0	CNF production (g)	R_w (g C/(g_{cat} h))
700	4	2.6	420	67.8	51.1	0.70	76.7	1.1
700	8	5.3	300	73.4	53.5	0.55	114.6	2.29
700	12	8	420	81	40.9	0.63	183.9	2.63
700	24	16	420	38.6	14.1	0.43	126.8	1.81
650	12	8	420	37.5	11.1	0.38	49.9	0.71
700	12	8	420	67.8	42.2	0.63	183.9	2.63
750	12	8	420	77.9	28.8	0.28	129.7	1.85
800	12	8	300	68.7	27.4	0.32	88.2	1.76
700	8	2	300	76.8	57.9	0.86	46.5	2.48
700	8	4	300	75.7	52.7	0.70	84.7	2.25
700	8	6	300	73.4	45.7	0.54	110.2	1.96

reaction rate measured after 5 h time on stream) is also shown in Table 1.

The initial hydrogen concentration and the average methane conversion were enhanced by increasing operating temperature and lowering space velocity and ratio u_o/u_{mf}. However, an increase in operating temperature, space velocity and the ratio u_o/u_{mf} provoked a decrease in the sustainability factor.

As regards the carbon product obtained, both the CNF yield and the average carbon deposition rate were highly dependent on the operating conditions used, currently passing through an optimum value. The highest catalyst performance in a fluidized reactor test was obtained at a temperature of 700 °C, a WHSV of 12 l/(g_{cat} h) and a u/u_{mf} of 8 for which operating conditions an average rate of 2.63 g C/(g_{cat} h) and a CNF yield of 184 g after 420 min time on stream were achieved.

3.2. Structural characterization

3.2.1. XRD

The structural properties of the deposited carbon in FBR tests at different operating conditions including the c parameter of the hexagonal unit cell, the L_c parameter and the degree of graphitization calculated from the Mering and Maire formula [25] are shown in Table 2.

The parameter c of the CNFs obtained in FBR tests under different operational conditions ranges from 0.6743 to 0.6789 nm, that according to Franklin's classification it corresponds to a turbostratic carbon structure [26]. The crystal domain size L_c and the degree of graphitization G are found in the range of 6.3–8 nm and 53–80%, respectively. As expected, an increase in the reaction temperature enhances the deposition of more-ordered CNFs, as derived from the increase in both the degree of graphitization and the crystal domain size, as well as in the reduction in the parameter c. The effect of the space velocity and the u_o/u_{mf} ratio was not significant. CNFs of similar structural properties but with a carbon production two orders of magnitude lower [27] were obtained in a fixed bed laboratory apparatus.

Table 2
Structural properties of the deposited carbon obtained in FBR tests at different operating conditions.

T (°C)	WHVS (l/(g_{cat} h))	u_o/u_{mf}	c (nm)	L_c (nm)	G (%)
700	4	2.6	0.6743	8.5	79.7
700	8	5.3	0.6752	8	74.4
700	12	8	0.6769	6.8	64.5
700	24	16	0.6754	7.8	73.3
650	12	8	0.6789	6.3	52.9
700	12	8	0.6769	6.8	64.5
750	12	8	0.6763	8.5	68
800	12	8	0.6781	7.7	57.6
700	8	2	0.6754	7.9	73.3
700	8	4	0.6767	7	65.7
700	8	6	0.6754	8.1	73.3

3.2.2. SEM and TEM characterization

In FBR tests catalyst particles are working in turbulent flow regime needed to prevent agglomeration problems in the CDM process, although this phenomenon may occur at higher u_o/u_{mf} ratio and it also depends on the catalyst used. Thus, CNFs are also subjected to high attrition rates which may provoke at least large changes in the morphology [10]. In order to elucidate the morphological and structural properties of the CNFs produced in the fluidized bed reactor, a detailed study by means of SEM and TEM has been conducted. The morphological appearance of samples obtained at different operating conditions in fluidized bed reactor tests using the $NiCu/Al_2O_3$ catalyst showed that most of the carbon is deposited as nanofibers.

Fig. 1 shows representative SEM images of samples obtained in FBR tests using the $NiCu/Al_2O_3$ catalyst at WHSV of 12 l/(g_{cat} h) and two reaction temperatures of 700 °C (Fig. 1a) and 800 °C (Fig. 1b). The sample obtained at 700 °C clearly shows the presence of CNFs a few nanometers in diameter and some micrometers in length (the exact length of the CNF cannot be quantified), although they coexist with fibers of higher diameter (ca. 500 nm). On the other hand, at 800 °C, some carbon nanofibres it seems to coexist with carbon in the form of uniform coatings encapsulating some catalyst particles. In a previous work [27] it was shown that the increase in reaction temperature leads to the suppression of the carbon growth in form of nanofiber, being predominant the formation of encapsulating carbon (which eventually deactivate the nickel particles), resulting in the increase in the structural degree of order for samples obtained at higher temperatures, as pointed out from the XRD study.

Similarly, Fig. 2 shows two SEM images of samples obtained in FBR tests at 700 °C using two different space velocities of 12 l/(g_{cat} h) (Fig. 2a) and 24 l/(g_{cat} h) (Fig. 2b). Even at the highest space velocities the presence of carbon nanofibers is clearly shown revealing that in the CDM carbon is usually deposited as CNFs despite the turbulent flow prevailing in a FBR.

Fig. 3 shows TEM images of CNFs obtained in FBR tests at 700 and 800 °C (Fig. 3a and b, respectively). In both cases, the respective carbon nanofibers had diameters of ca. 20–30 nm, and they show the graphenes with an inclination of some degrees to respect the fiber axis forming fishbone like structure. This angle is related to the (1 1 1) nickel crystallites plane, resulting in the epitaxial growth encountered with CNF. Moreover, the characteristic graphene angle with the fiber axis is slightly increased with the increase in the reaction temperature, from 40 to 46° for the samples obtained at 700 and 800 °C, respectively. Additionally, the overall order degree of the graphitic structure of the CNFs obtained

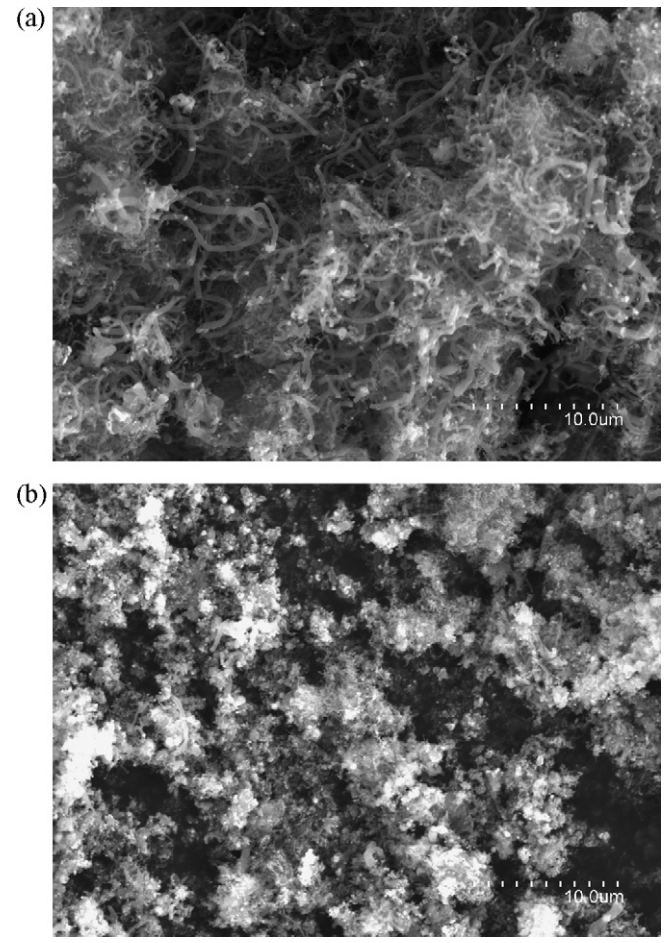

Fig. 1. SEM images of samples obtained in FBR tests at VHSV of 12 l/(g_{cat} h) and different reaction temperatures: (a) 700 °C and (b) 800 °C.

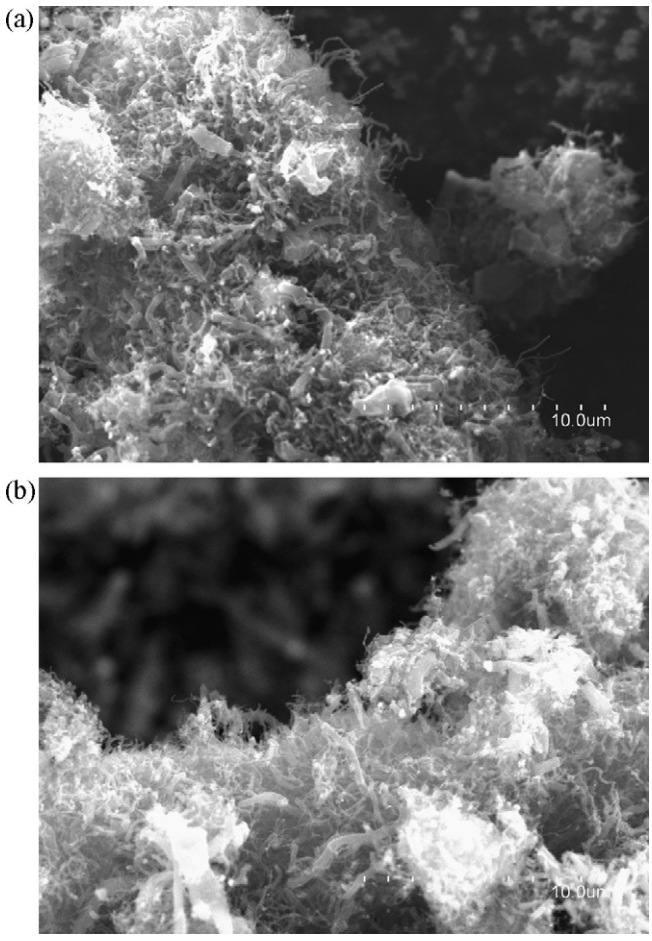

Fig. 2. SEM images of samples obtained in FBR tests at *T* of 700 °C and different space velocities: (a) 8 l/(g_{cat} h) and (b) 24 l/(g_{cat} h).

corresponds to a turbostratic carbon in complete agreement with the XRD study.

3.2.3. Temperature-programmed oxidation

TPO is a useful tool for quantifying the different carbon species present on a sample, given that the reactivity of carbon with oxygen is highly dependent on the structural order of the graphenes, i.e., amorphous and/or graphitic nature [28]. Fig. 4 shows the cumulative weight loss curves obtained in a thermal scanning of samples obtained in FBR tests at 700 and 800 °C and WHSV of 12 l/(g_{cat} h). Given that the more pronounced differences were observed between these two samples, the other TPO curves have been omitted in order to allow a better and easier comparison, avoiding curves overlapping. The TPO profile of sample obtained at 800 °C is a curve showing two slopes: one at temperatures lower than 575 °C, and other at temperatures higher than 575 °C. These two slopes suggest the presence in the sample of two kinds of carbon with different structural order: the first one burning at lower temperature with a less-ordered structure and a second one burning at higher temperature with higher structural order. According to the previous SEM and TEM studies in this sample there is a less-ordered carbon structure in the form of CNFs and another more-ordered carbon in the form of uniform coatings. The two carbon forms found in the TPO profile has to be assigned to these different carbon forms. On the other hand, the TPO profile obtained from the sample at 700 °C is a curve with a single slope assigned to a single carbon form. Again, the SEM and TEM studies showed clearly that in this sample there was a single carbon type in the form of less-ordered nanofibers.

Table 3 shows data extracted from the respective TPO profiles of samples obtained from FBR tests at different operating conditions. Table 3 includes the maximum oxidation temperature ($T_{r_{max}}$), which is defined as the temperature at which the oxidation rate reaches a maximum, and the oxidation rate at such temperature (r_{max}). It is observed that as the reaction temperature was increased, the $T_{r_{max}}$ also did indicating that the carbon produced at higher reaction temperatures had a higher structural order, in complete agreement with XRD and TEM studies. However, the space velocity and the ratio u_o/u_{mf} have an opposite effect than

Table 3
Maximum oxidation temperature ($T_{r_{max}}$) and the oxidation rate at such temperature (r_{max}) obtained from the respective TPO profiles.

T (°C)	WHVS (l/(g_{cat} h))	u_o/u_{mf}	$T_{r_{max}}$ (°C)	r_{max} (%/°C)
700	4	2.6	542	2.11
700	8	5.3	545	1.28
700	12	8	508	1.01
700	24	16	526	0.98
650	12	8	494	1.04
700	12	8	508	1.01
750	12	8	529	1.16
800	12	8	559	1.53
700	8	2	560	1.72
700	8	4	535	2
700	8	6	507	1.14

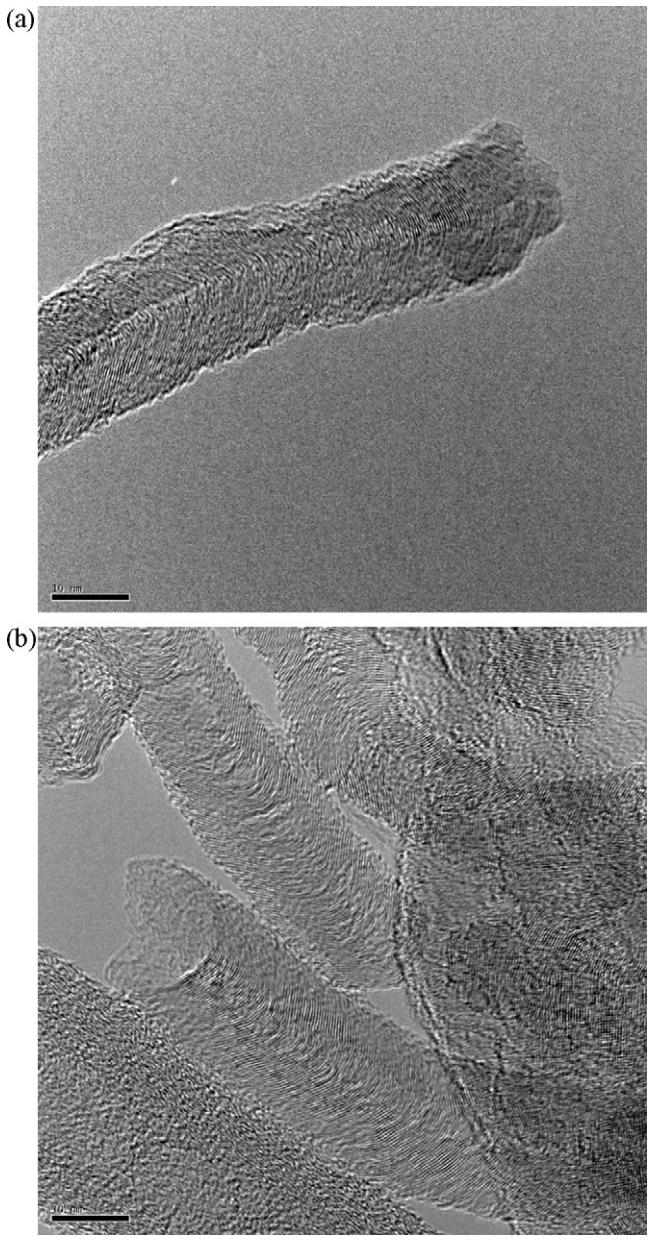

Fig. 3. TEM images of samples obtained at VHSV of 12 l/(g_{cat} h) and different reaction temperatures: (a) 700 °C and (b) 800 °C.

the temperature and, for example, less-ordered carbon is produced at higher space velocities. This feature can be explained in terms of hydrogen partial pressure at the reactor outlet. In previous works it was shown that high hydrogen partial pressures (corresponding to high methane conversions in the CDM) lead to more-ordered carbons depositions [29]. Thus, a plausible explanation is that as space velocity is increased, methane conversion and therefore hydrogen partial pressure is reduced (Table 1), thus explaining the lower structural degree of order observed for the CNF obtained at high space velocities.

3.3. Textural properties

The textural properties of the fresh catalyst, as well as those obtained for the samples obtained in the FBR tests at different operating conditions are shown in Table 4. Specific surface area and pore volume of the fresh catalyst had values of 80 m^2/g and 0.24 cm^3/g, respectively. The specific surface areas of the samples after reaction

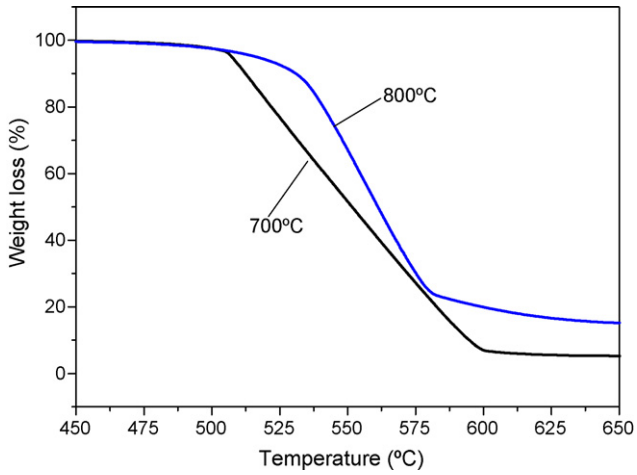

Fig. 4. TPO profiles of samples obtained in FBR tests at temperatures of 700 and 800 °C and a space velocity of 12 l/(g_{cat} h).

range from 66 to 128 m^2/g and the isotherm shapes correspond to mesoporous materials with mesopores mainly located in the CNFs core and in defective graphenes as deduced from the TEM study. According to Suelves et al. [2], catalyst deactivation cannot be associated to pore plugging, since the specific surface areas of the used catalysts does not correlate with their state, active or inactive. Additionally, there was no relationship between the specific surface area of the fresh catalysts and the surface area of the deposited carbon.

Samples obtained in FBR tests at low reaction temperatures, high space velocities and high u_o/u_{mf} ratios show the highest specific surface areas as expected from the formation of low-order carbon nanofibers. Pore volume data of these samples takes values ranging from 0.25 to 0.39 cm^3/g, showing similar tendencies to that of the surface area.

Regarding the appearance of the nanofibrous carbon after performing the reaction tests, the fixed bed density, the final bed height, the particle size distribution as well as the ratio of gas flow velocity, u_o, to the minimum fluidization velocity for the carbonaceous product at the final stage of the runs, $u_{mf\text{-}end}$ have been determined and they are shown in Table 5. The calculation of the $u_{mf\text{-}end}$ has been carried out by using the equation of Wen and Yu [24], using as constant those proposed by Adánez et al. for carbonaceous materials [30].

The influence of the operational conditions on the bulk density and the mean particle size were not determinant. Bulk densities of the carbonaceous sample after reaction tests were in the range 200–500 kg/m^3, lower than that obtained for the fresh catalyst (730 kg/m^3). The mean particle size of the carbonaceous product

Table 4
Textural properties obtained by N_2 adsorption at 77 K of the samples obtained in FBR tests at different operating conditions.

T (°C)	WHVS (l/(g_{cat} h))	u_o/u_{mf}	S_{BET} (m^2/g)	S_{meso} (m^2/g)	V_p (cm^3/g)
Fresh catalysts			80	70	0.24
700	4	2.6	82	75	0.19
700	8	5.3	72	67	0.23
700	12	8	102	94	0.25
700	24	16	94	88	0.26
650	12	8	128	111	0.25
700	12	8	102	94	0.25
750	12	8	66	61	0.18
800	12	8	79	74	0.20
700	8	2	82	76	0.19
700	8	4	88	77	0.21
700	8	6	94	86	0.23

Table 5
Fixed bed density, final bed height, mean particle size and the minimum fluidization velocity of the carbonaceous product at the end of the CDM runs.

T (°C)	WHVS (l/(g_{cat} h))	u_o/u_{mf}	Density (kg/m^3)	Final bed height (cm)	Mean particle size (μm)	$u_o/u_{mf\text{-}end}$
	Fresh catalyst		730	–	150	
700	4	2.6	318	7.3	59.7	17.7
700	8	5.3	476	7.3	233.3	1.6
700	12	8	400	13.9	181.3	4.6
700	24	16	519	7.4	235.4	4.2
650	12	8	191	7.9	14.3	
700	12	8	400	13.9	181.3	4.6
750	12	8	503	7.8	286.2	1.6
800	12	8	425	6.3	201.6	4.2
700	8	2	383	3.7	193.1	1.1
700	8	4	346	7.4	128.4	5.4
700	8	6	354	9.4	143.5	6.3

were in the same range for that obtained for the fresh catalysts (150 μm), although larger particle size distribution was found, with values ranging from 50 to 400 μm.

As regards the process evolution during the CDM tests, no defluidization problems were observed during the entire duration of the runs. However, it is interesting to notice that the ratio $u_o/u_{mf\text{-}end}$ calculated according to the morphological characteristics of the carbon produced at the end of the reaction tests (Table 5) changes substantially in comparison to those values calculated for the fresh catalyst (u_o/u_{mf}) due to the changes occurred in the catalysts as the reaction proceed. In most of the tests performed the $u_o/u_{mf\text{-}end}$ ratio is reduced about a 50% of the u_o/u_{mf} ratio, although in some cases the reduction is much more pronounced. However, other tests preformed showed similar values of u_o/u_{mf} and $u_o/u_{mf\text{-}end}$. Thus, this point should be very carefully taken into account in order to accomplish a future scale-up of the process. Additionally, large variations in the temperature were neither observed.

In order to confirm the correct fluidization of the bed of particles as the reaction proceeds, a typical pressure drop profile corresponding to the test carried out at 750 °C and 12 l/(g_{cat} h), which had a u_o/u_{mf}: 1.6, is shown in Fig. 5. It can be observed that the increase in the measured pressure drop can be related to the mass gained due to carbon deposition onto the catalysts particles (right axis). Thus, the bed weight at the end of the tests, 140 g, corresponds to a final pressure drop of 3.9 mbar, close to that expected to the maximum theoretical pressure drop, 4.2 mbar ($\Delta p_{max} = W/S$, where W is the mass of carbon product (g) and S is the cross-sectional area in cm^2).

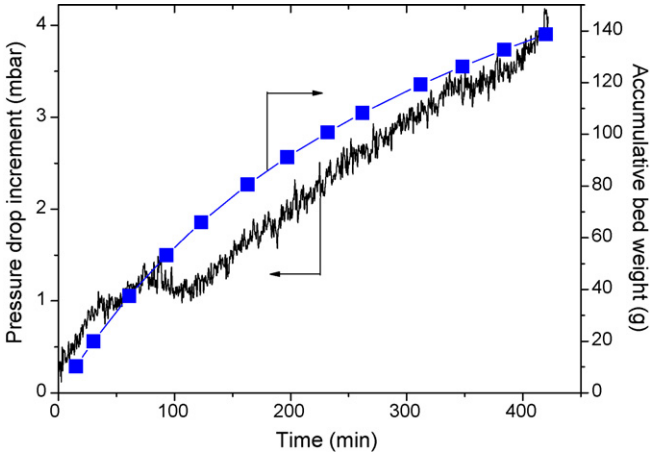

Fig. 5. Pressure drop profile (left axis) and accumulative bed weight (right axis) versus time on stream, corresponding to the test carried out at 750 °C and 12 l/(g_{cat} h).

3.4. Comparative study of the properties of the filamentous carbon obtained at different production scales and contacting mode

In previous works carried out by our research group it was shown the viability of producing large quantities of carbon nanofibers using nickel based catalysts in a FBR [17,19,20]. This work presents the characterization of carbon forms obtained under different operating conditions. The results previously mentioned revealed that high quality CNFs can be produced by selecting carefully the experimental conditions used. However, some of the main variables which have to be taken into account when a future industrial scale-up, that is, space velocity and ratio u_o/u_{mf}, affect not only the methane conversion but also the structural and textural properties of the CNFs produced.

In order to evaluate the quality of large-scale CNFs produced in a FBR, a comparison of the textural and structural properties of the CNFs produced under identical operating conditions, but changing the reactor type and the contacting mode (fixed bed reactor) is shown in Table 6. Data from the fixed bed reactor test have been taken from [27]. Additionally, data regarding the catalytic performance in the CDM in terms of initial hydrogen concentration ($H_{2,0}$), average methane conversion (χ_{CH_4}), sustainability factor (r_5/r_0) and carbon average deposition rate (R_w) are also shown in Table 6.

The catalyst performance in the FBR is substantially lower that that obtained in the FBR, as it can be observed in Table 6. For instance, carbon average deposition rate was found to be 7.02 and 1.81 g/(g_{cat} h) in the fixed bed and in the FBR, respectively. Unlike fixed bed operation, in fluidized bed operation, it is assumed that all

Table 6
A comparison of the catalytic performance (hydrogen concentration ($H_{2,0}$), average methane conversion (χ_{CH_4}), sustainability factor (r_5/r_0) and carbon average deposition rate (R_w)), textural and structural properties of CNFs obtained in a fixed bed reactor and fluidized bed reactor at the same operating conditions of 700 °C and 24 l/(g_{cat} h).

		Fixed bed	Fluidized bed
Catalyst performance	$H_{2,0}$ (vol.%)	73.2	38.5
	χ_{CH_4}	54.61	14.1
	r_5/r_0	0.72	0.58
	R_w (g C/(g_{cat} h))	7.02	1.81
N_2 adsorption	S_{BET} (m^2/g)	93	94
	S_{meso} (m^2/g)	84	88
	V_p (cm^3/g)	0.26	0.27
XRD	c (nm)	0.6765	0.6754
	L_c (nm)	7.8	7.8
	G (%)	66.9	73.3
TPO	$T_{r_{max}}$ (°C)	581	526
	r_{max} (%/°C)	1.84	0.98

gas in excess of that required for the minimum fluidization passes through the beds as bubbles. This fact can explain the lower efficiency accounted in the FBR.

Both the structural from XRD and the textural from N_2 adsorption data are very similar in both types of reactors. Additionally, the data extracted from the TPO curves ($T_{r_{max}}$ and r_{max}) showed that carbon obtained in the fixed bed reactor is less reactive toward oxygen, than the carbon obtained in the FBR.

The morphological appearance of samples obtained in both experimental apparatus using the $NiCu/Al_2O_3$ catalyst showed that most of the carbon had a similar morphology. As an example in [27] can be found some representative images of the CNF obtained in the fixed bed reactor using the same $NiCu/Al_2O_3$ catalyst.

Despite the lower catalytic performance obtained under the same operational conditions in the FBR in comparison to the fixed bed reactor, the FBR test prevent the appearance of agglomeration in the reactor bed, as it has been stated in Section 3.3. Thus, the scale-up of the CNF production process in a FBR has been accomplished satisfactorily, not only in terms of methane conversion and increase in CNF production capability, but also in terms of CNF quality. This fact renders the possibility of obtaining CNF in the hundreds of grams scale with physico-chemical properties analogous to those obtained in the fixed bed reactor.

4. Conclusions

An investigation of the influence of the operating conditions (temperature, space velocity and the ratio u_o/u_{mf}) on the structural and textural properties of the carbon produced in a CDM process has been carried out in a FBR. Results showed that the deposited carbon appears mainly as long CNFs emerging from the nickel particles exhibiting a typical fishbone structure. The CNFs present specific surface areas values ranging from 80 to 130 m^2/g due to the presence of mesopores mostly located between disorder graphenes. The increase in the reaction temperature resulted in carbons with higher structural order although the presence of more-ordered encapsulating carbon only occurs at higher temperatures. The effect of the space velocity and the u_o/u_{mf} ratio seems to be opposite to that of temperature and less-ordered carbon is produced at higher space velocities and higher u_o/u_{mf} ratios.

It has been proven that a FBR is a suitable configuration to carry out the CDM process allowing the production of CNFs with physico-chemical properties analogous to the ones obtained in a fixed bed reactor preventing the appearance of agglomeration problems.

Acknowledgements

This work was carried out with financial support from the Spanish CDTI (Project CENIT SPHERA), GAS NATURAL, S.A and the Spanish MICINN (Proyecto ENE2008-06516, Plan Nacional de Energía-FEDER).

References

[1] N.Z. Muradov, T.N. Vezirolu, From hydrocarbon to hydrogen–carbon to hydrogen economy, Int. J. Hydrogen Energy 30 (2005) 225–237.
[2] I. Suelves, M.J. Lázaro, R. Moliner, B.M. Corbella, J.M. Palacios, Hydrogen production by thermo catalytic decomposition of methane on Ni-based catalysts: influence of operating conditions on catalyst deactivation and carbon characteristics, Int. J. Hydrogen Energy 30 (2005) 1555–1567.
[3] L. Calvillo, M. Gangeri, S. Perathoner, G. Centi, R. Moliner, M.J. Lázaro, Effect of the support properties on the preparation and performance of platinum catalysts supported on carbon nanofibers, J. Power Sources 192 (2009) 144–150.
[4] G.G. Tibbetts, M.L. Lake, K.L. Strong, B.P. Rice, A review of the fabrication and properties of vapour-grown carbon nanofiber/polymer composites, Compos. Sci. Technol. 67 (2007) 1709–1718.
[5] C.A. Bessel, K. Laubernds, N.M. Rodríguez, R.T.K. Baker, Graphite nanofibers as an electrode for fuel cell applications, J. Phys. Chem. 105 (2001) 1115–1118.
[6] A.B. Garcia, I. Cameán, I. Suelves, J.L. Pinilla, M.J. Lázaro, J.M. Palacios, R. Moliner, The graphitization of carbon nanofibers produced by the catalytic decomposition of natural gas, Carbon 47 (2009) 2563–2570.
[7] S.G. Zavarukhin, G. Kuvshinov, The kinetic model of nanofibrous carbon from CH_4–H_2 mixture over a high-loaded nickel catalyst with consideration for the catalyst deactivation, Appl. Catal. A: Gen. 272 (2004) 219–227.
[8] K.P. De Jong, J.W. Geus, Carbon nanofibers: catalytic synthesis and applications, Catal. Rev. Sci. Eng. 42 (2000) 481–510.
[9] J.L. Pinilla, R. Utrilla, M.J. Lázaro, I. Suelves, R. Moliner, J.M. Palacios, A novel rotary reactor configuration for simultaneous production of hydrogen and carbon nanofibers, Int. J. Hydrogen Energy 34 (2009) 8016–8022.
[10] S.L. Pirard, J.P. Pirard, C. Bossuot, Modeling of a continuous rotary reactor for carbon nanotube synthesis by catalytic chemical vapor deposition, AIChE J. 55 (2009) 675–683.
[11] C.H. See, A.T. Harris, A review of carbon nanotube synthesis via fluidized-bed chemical vapour deposition, Ind. Eng. Chem. Res. 46 (2007) 997–1012.
[12] R. Philippe, A. Morançais, M. Corrias, B. Caussat, Y. Kihn, P. Kalck, D. Plee, P. Gaillard, D. Bernard, P. Serp, Catalytic production of carbon nanotubes by fluidized bed CVD, Chem. Vapor Depos. 13 (2007) 447–457.
[13] V.N. Parmon, G.G. Kuvshinov, V.A. Sadykov, V.A. Sobyamon, New catalysts and catalytic processes to produce hydrogen and syngas from natural gas and other light hydrocarbons, Stud. Surf. Sci. Catal. 119 (1998) 677–684.
[14] W. Qian, T. Liu, Z. Wang, F. Wei, Z. Li, G. Luo, Y. Li, Production of hydrogen and carbon nano tubes from methane decomposition in a two-stage fluidized bed reactor, Appl. Catal. A: Gen. 260 (2004) 223–228.
[15] N. Shah, S. Ma, Y. Wang, G.P. Huffman, Semi-continuous hydrogen production from catalytic methane decomposition using a fluidized-bed reactor, Int. J. Hydrogen Energy 32 (2007) 3315–3319.
[16] P. Ammendola, R. Chirone, G. Ruoppolo, G. Russo, Production of hydrogen from thermo-catalytic decomposition of methane in a fluidized bed reactor, Chem. Eng. J., (2009) doi:10.1016/j.cej.2009.03.048.
[17] J.L. Pinilla, R. Moliner, I. Suelves, M.J. Lázaro, Y. Echegoyen, J.M. Palacios, Production of hydrogen and carbon nanofibers by thermal decomposition of methane using metal catalysts in a fluidized bed reactor, Int. J. Hydrogen Energy 32 (2007) 4821–4829.
[18] C. Vahlas, B. Caussat, P. Serp, G.N. Angelopoulus, Principles and applications of CVD powder technology, Mater. Sci. Eng. R 53 (2006) 1–72.
[19] J.L. Pinilla, I. Suelves, M.J. Lázaro, R. Moliner, J.M. Palacios, Parametric study of the decomposition of methane using a $NiCu/Al_2O_3$ catalyst in a fluidized bed reactor, Int. J. Hydrogen Energy, (2009) doi:10.1016/j.ijhydene.2009.10.008.
[20] I. Suelves, J.L. Pinilla, R. Utrilla, M.J. Lázaro, R. Moliner, J.M. Palacios, Methane decomposition using Ni-based catalyst for hydrogen production in a fluidized bed reactor. Hydrogen systems and materials for sustainability, in: C.M. Rangel, G. Spazzafumo (Eds.), Proceedings HYPOTHESIS VIII, Lisboa, April 1–3, 2009.
[21] Y. Echegoyen, I. Suelves, M.J. Lázaro, R. Moliner, J.M. Palacios, Hydrogen production by thermocatalytic decomposition of methane over Ni–Al and Ni–Cu–Al catalysts: effect of calcination temperature, J. Power Sources 169 (2007) 150–157.
[22] I. Suelves, M.J. Lázaro, R. Moliner, Y. Echegoyen, J.M. Palacios, Characterization of NiAl and NiCuAl catalysts prepared by different methods for hydrogen production by thermo catalytic decomposition of methane, Catal. Today 116 (2006) 271–280.
[23] J.L. Pinilla, I. Suelves, M.J. Lázaro, R. Moliner, J.M. Palacios, Influence of nickel crystal domain size on the behaviour of Ni and NiCu catalysts for the methane decomposition reaction, Appl. Catal. A: Gen. 363 (2009) 199–207.
[24] C. Wen, Y. Yu, A generalized method for predicting minimum fluidization velocity, AIChE J. 12 (1966) 610–612.
[25] J. Maire, J. Mering, Graphitization of soft carbons, in: P.L. Walker (Ed.), Chemistry and Physics of Carbon, vol. 6, Marcel Dekker, New York, 1970, pp. 125–190.
[26] R.E. Franklin, The structure of graphitic carbons, Acta Crystallogr. 4 (1951) 253.
[27] I. Suelves, J.L. Pinilla, M.J. Lázaro, R. Moliner, J.M. Palacios, Effects of reaction conditions on hydrogen production and carbon nanofiber properties generated by methane decomposition in a fixed bed reactor using a NiCuAl catalyst, J. Power Sources 192 (2009) 35–42.
[28] D. González, O. Altin, S. Eser, A.B. Garcia, Temperature-programmed oxidation studies of carbon materials prepared from anthracites by high temperature treatment, Mater. Chem. Phys. 101 (2007) 137–141.
[29] J.L. Pinilla, I. Suelves, M.J. Lázaro, R. Moliner, J.M. Palacios, Activity of NiCuAl catalyst in methane decomposition studied using a thermobalance and the structural changes in the Ni and the deposited carbon, Int. J. Hydrogen Energy 33 (2008) 2515–2524.
[30] J. Adánez, J.C. Abadanes, Minimum fluidization velocities of fluidized-bed coal-combustion solids, Powder Technol. 67 (1991) 113–119.